Interfaces: Adsorption, Reactions, Films, Forces, Measurement Techniques, Charge Transfer, Electrochemistry, Electrocatalysis, Energy Production and Storage

N-doped TiO photocatalyst coatings synthesized by a cold atmospheric plasma

Qianqian Chen, Alp Ozkan, Basab Chattopadhyay, Kitty Baert, Claude Poleunis, Alisson Tromont, Rony Snyders, Arnaud Delcorte, Herman Terryn, Marie-Paule Delplancke-Ogletree, Yves H. Geerts, and François Reniers

Langmuir, **Just Accepted Manuscript** • DOI: 10.1021/acs.langmuir.9b00784 • Publication Date (Web): 10 May 2019

N-doped TiO_2 photocatalyst coatings synthesized by a cold atmospheric plasma

Qianqian Chen [1*], Alp Ozkan [1], Basab Chattopadhyay [2], Kitty Baert [3], Claude Poleunis [4], Alisson Tromont [5], Rony Snyders [5, 6], Arnaud Delcorte [4], Herman Terryn [3], Marie-Paule Delplancke-Ogletree [7], Yves H. Geerts [2] , François Reniers [1*]

[1] *Chemistry of Surfaces, Interfaces, and Nanomaterials, Faculté des Sciences, Université libre de Bruxelles, ULB Boulevard du Triomphe, Brussels 1050, Belgium*

[2] *Laboratoire de chimie des polyméres, Faculté des Sciences, Université Libre de Bruxelles, ULB Boulevard du Triomphe, Brussels 1050, Belgium*

[3] *Research Group Electrochemical and Surface Engineering, Vrije Universiteit Brussel, Pleinlaan 2, 1050 Brussels, Belgium*

[4] *Institute of Condensed Matter and Nanosciences, Université Catholique de Louvain, 1348 Louvain-la-Neuve, Belgium*

[5] *Materia Nova Research Center, Parc Initialis, B-7000 Mons, Belgium*

[6] *ChIPS, CIRMAP, Université de Mons, 23 Place du Parc, B-7000 Mons, Belgium*

[7] *4MAT, CP 165/63, Université Libre de Bruxelles, 50 Av. F.D. Roosevelt, B-1050 Brussels, Belgium*

* Email: Qianqian.Chen@ulb.ac.be; Fax: + 32-2-650-2934; Tel: + 32-2-650 2943

Email: freniers@ulb.ac.be; Fax: + 32-2-650-2934; Tel: +32-2-650-3116

Abstract

This work presents a simple, fast (20 minutes treatment), inexpensive and highly efficient method to synthesize nitrogen doped titanium dioxide (N-TiO_2) as an enhanced visible light photocatalyst.

In this study, N-TiO_2 coatings were fabricated by atmospheric pressure dielectric barrier discharge (DBD) at room temperature. The composition and the chemical bonds of the TiO_2 and N-TiO_2 coatings were characterized by X-ray photoelectron spectroscopy (XPS) and time of flight secondary ion mass spectroscopy (ToF-SIMS). The results indicate that the nitrogen element has doped the TiO_2 lattice, which was further confirmed by Raman spectroscopy and Grazing Incidence X-ray Diffraction (GIXRD). The doping mechanism was investigated using OES to study the plasma properties under different conditions. It suggests that the NH radicals play a key role in doping TiO_2. The concentration of nitrogen in the N-TiO_2 coatings can be controlled by changing the concentration of NH_3 in the plasma or the applied power to adjust the concentration of NH radicals in the plasma. The bandgap of N-TiO_2 was reduced after NH_3/Ar plasma treatment from 3.25 to 3.18 eV. Consequently, the N-TiO_2 coating showed an enhanced photocatalytic activity under white light-emitting-diode (LED) irradiation. The photocatalytic degradation rate for N-TiO_2 coating was about 1.4 times higher than that of the undoped TiO_2 coating.

Keywords: N-doped TiO_2; atmospheric pressure; room temperature; dielectric barrier discharge; NH_3/Ar discharge; photocatalytic property

Introduction

Titanium dioxide (TiO_2) is one of the most promising sustainable photocatalysts for pollutants removal [1-3]. However, the wide band gap (~ 3.2 eV) of TiO_2 limits its excitation region in the ultraviolet (UV) range (wavelength $\lambda < 388$ nm), which only constitutes about 5% of the solar spectrum energy [2]. With the purpose of utilization for the application of TiO_2 in a wider solar spectrum, enhancing the energy absorption to the visible light range is an interesting approach to improve its properties.

In recent years, visible-light-active TiO_2 materials that doped with nonmetal impurities is regarded as one of the most promising techniques to reduce the band gap of TiO_2 [3-5]. Among several dopants, based on the electronic band structures calculation [5-7], nitrogen (N) has been identified as a preferred candidate. The formation of a substitution N 2p band above the O 2p valence band narrows the band gap of TiO_2 and the optical absorption of doped TiO_2 shifts to the visible light region [5,8-10]. Besides, compared with other nonmetals elemental doping, N-doped TiO_2 materials show higher enhanced photocatalytic activity and stronger optical absorption in the visible light irradiation [9].

Several methods are used for the preparation of N-doped TiO_2 [9-13], including physical methods and chemical methods. N-TiO_2 thin films were successfully synthesized by high power impulse magnetron sputtering plasma at a pressure of 0.93 Pa, and for a treatment time of 120 min. The authors showed that the energy gap of the TiO_2 film was reduced from 3.45 to 3.40 eV after doping [11]. Yang and coworkers [9] prepared N doped TiO_2 by the solvothermal method, which showed enhanced absorption in the visible light region, and exhibited a high photocatalytic activity for the degradation of

model dyes. It had been shown that N doping, with Ti^{3+} ions and oxygen vacancies, made contributions to the visible light absorption of N doped TiO_2. B. Kosowska and coworkers [13] investigated N-doped TiO_2 catalysts by calcination of hydrated amorphous TiO_2 particles in gaseous NH_3 atmosphere at 100-800 °C for 4 h. The modified TiO_2 exhibited visible light photocatalytic activity with a reduced band gap of 2.64 eV. Even though the above-mentioned modification methods show that nitrogen has doped TiO_2 successfully, the recognized drawbacks of these methods are that they are time and energy consuming.

Plasma related techniques are environment-friendly and energy-saving methods, that involve high-energy species such as electrons, atoms, and radicals for surface modification and chemistries to impart a variety of physiochemical properties to various materials [14,15]. The dielectric barrier discharge (DBD) plasma, one of the non-thermal plasmas characterized by a high electron temperature (10^4 - 10^5 °C) but a low bulk gas temperature (as low as room temperature), can be operated at atmospheric pressure, which is a promising technique for catalyst modification. While high temperature and solvent-based treatments are required based on the methods listed above, plasma-assisted doping is conducted at a relatively low temperature without changing the morphology or the structure of TiO_2. Some recent studies have shown a positive effect of plasma treatment on surface modifications [14-17]. Since NH_3 plasma consists of various nitriding species and excited hydrogen [16,18], NH_3 plasma irradiation on the surface of TiO_2 powders induced an improvement of the photocatalytic properties under visible light [14]. Plasma nitridation of tool steel under atmospheric pressure was

performed by $Ar/N_2/H_2$ DBD, resulting in the formation of a uniform nitride layer and a twofold surface hardness compared with the original one [15]. Multiwall carbon nanotubes (MWCNTs) were modified using a microwave-excited NH_3/Ar plasma [19]. Nitrogen-containing groups were introduced on the surfaces of the MWCNTs and the hydrophilicity of the modified MWCNTs was improved.

In the present study, we propose a simple method to synthesize N-doped TiO_2 materials at room temperature involving DBD under atmospheric pressure. This study aims to: (i) introduce nitrogen into the TiO_2 lattice by a NH_3/Ar mixture plasma treatment and investigate the evolution of the compositions and the structures; (ii) study the doping mechanisms of TiO_2 by a NH_3/Ar plasma by Optical Emission Spectroscopy (OES) and (iii) estimate the photocatalytic performance through the degradation of methylene blue (MB) underexposure of white light-emitting-diode (LED) lamps.

Experimental part

Preparation of TiO_2 and N-TiO_2 films

The plasma reactor (shown in Figure 1) is a homemade atmospheric pressure DBD reactor. The DBD reactor chamber is made of glass with a diameter of 210 mm and a wall thickness of 6 mm. Two copper electrodes of 75 mm in diameter are inside the chamber and the plasma is generated in between. Each electrode is covered with a 3 mm thick alumina barrier and the electrodes gap is 3 mm. An AFS G10S-V AC power supply, operating at 2.7 kHz is connected to the high voltage electrode. A half piece of the silicon wafer ((001), 5.08 cm diameter) is used as the substrate, which is cleaned by isopropanol and methanol successively before each deposition. Prior to deposition, the

chamber is pumped down to a pressure of 4.5 Torr and then backfilled with Ar to atmospheric pressure to avoid air contamination. TTIP (titanium isopropoxide, 97%, Sigma-Aldrich), heated at 343 K, is used as a precursor for titanium and is introduced directly into the chamber as a vapor carried by an Ar flux. The pipeline between the bubbler and the chamber is heated at 373 K to prevent any condensation of the precursor on it. Moreover, the temperature of the substrate is set at 423 K (measured by an infrared thermometer before and after the deposition). During the deposition processes, the gas flow rate is 2 slm for the carrier gas (Ar) and 0.5 slm for O_2. The applied power is 30 W and the deposition time is 10 min. According to our earlier studies, the as-deposited TiO_2 films are amorphous [20]. Therefore, a heat treatment (annealing in air) at 723 K for 2 hours is used to get the crystalline TiO_2 films. This preparation method has been described in [20].

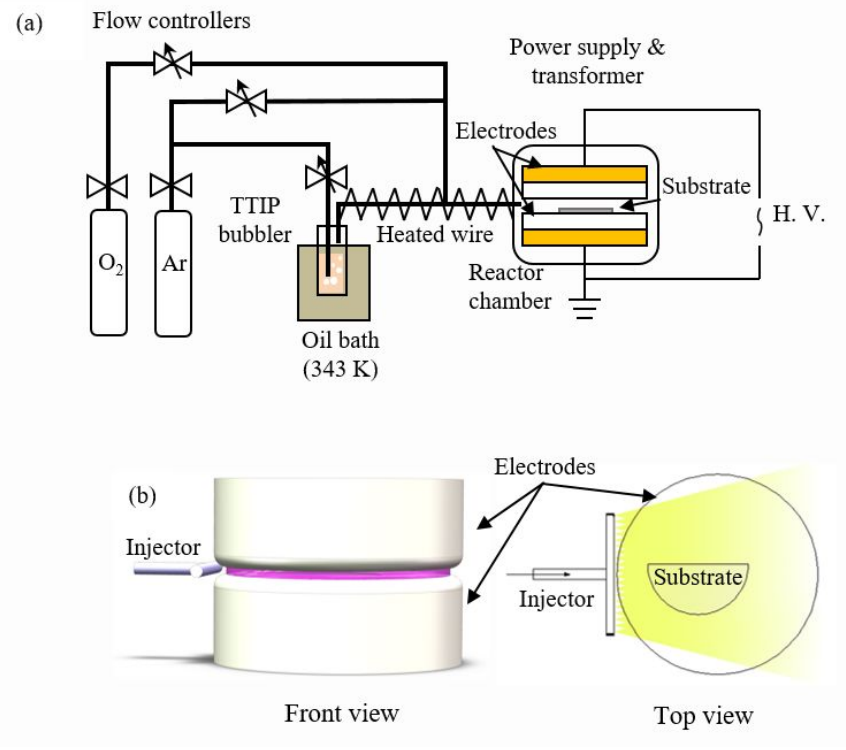

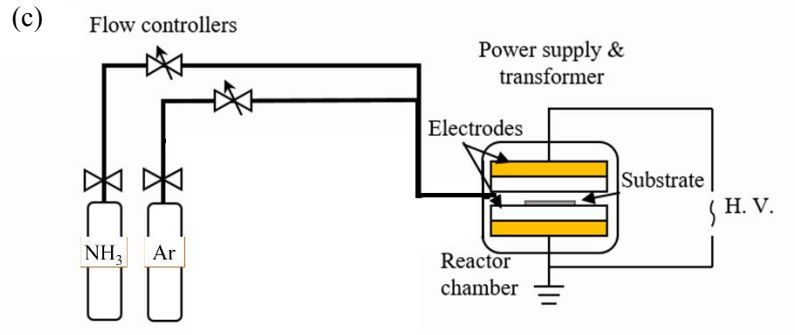

Fig. 1 Schematic of (a) the experimental setup for the deposition of TiO_2 films; (b) the detailed designs of the DBD reactor systems; (c) the experimental setup for doping.

The annealed TiO_2 films are used to prepare N-doped TiO_2 films using the same system that is used for deposition. The annealed TiO_2 films are put onto the middle of the bottom electrode, which is used without any heating, and exposed to an Ar/NH_3 DBD-plasma. Prior to any treatment, the chamber is pumped down to remove air and then backfilled with Ar. Afterward, 2 slm of Ar and NH_3 are injected in the chamber. Then, the DBD-plasma is lighted up at room temperature. After 20 min treatment, the resulting coating (denoted as N-TiO_2) is obtained. To study the doping mechanism, different concentrations of NH_3 (the flow rate ratio of NH_3 to Ar varied from 0.5 – 5%) and different applied power (30 – 100 W) was used.

Characterization

XPS analysis is performed on PHI 5600ci spectrometer with an Mg X-ray source (Kα = 1253.6 eV) under vacuum about 10^{-9} Torr at 200 W operated at 14 kV. Both survey scans (187.85 eV pass energy, with 0.25 eV/step, 3 sweeps) and high-resolution scans (23.5 eV pass energy, with 0.05 eV/step, 5 sweeps) are recorded. The spectra are calibrated according to the C1s peak at 284.6 eV as a reference. The Casa XPS software

is used for data interpretation using a Shirley background. The sensitivity coefficients are from the manufacturer's handbook: $S_C = 0.205$, $S_O = 0.63$, $S_N = 0.38$, and $S_{Ti} = 1.1$. For XPS analysis, some samples are subjected to Ar^+ sputtering to remove the surface contamination. Ar sputtering is performed using a 4 keV beam rastered over 2*2 mm^2. For the depth profile acquired in this study, time of flight secondary ion mass spectra (ToF-SIMS) was recorded using an IonToF instrument (GmbH, Münster, Germany). 1 keV Cs^+ with 100 nA current is used to create an area of 500 × 500 μm^2, and the middle 200 × 200 μm^2 is analyzed using pulsed 0.6 pA Bi^{3+} primary ion beam at 30 kV accelerating voltage. The positive secondary ion mass spectra are calibrated using C^+, TiO^+, TiN^+, and $TiON^+$. All data analyses are carried out using the software supplied by the instrument manufacturer, SurfaceLab.

The use of Grazing Incidence X-ray Diffraction (GIXRD, Rigaku Ultima IV diffractometer) to determine the crystallinity of the film. The GIXRD spectra are recorded at a constant incidence angle of 0.5° with Cu Kα (λ = 1.5418 Å) irradiation.

Raman microscopy (LabRAM HR Evolution, HORIBA Scientific), is also used to identify the crystallinity of the films. It is equipped with a multichannel air-cooled CCD detector (spectral resolution <1 cm^{-1}, lateral resolution 0.5 μm, axial resolution 2 μm), a solid-state laser corresponding to green light (532 nm) and works at 1.25 mW excitation with 10% filter.

The surface morphology and the film thickness of the deposited films are examined using a Scanning Electron Microscope (SEM, Hitachi SU 70) operating at 20 kV.

Optical Emission Spectroscopy (OES) diagnostics allow to determine and evaluate

some specific excited species in the plasma phase. It is performed with an Andor Shamrock-500i spectrometer (0.500 meter focal length, triple grating imaging) including an Andor DU420A-OE CCD camera.

Photocatalytic activity tests

Methylene blue (MB) is utilized as a model dye to evaluate the photocatalytic activity of the films. The degradation of MB is carried out by self-made equipment. White light-emitting-diode (LED) lamps (10 W, Philip) are used as the visible light source [21]. The distance between the LED lamps and the fluid level is kept as 150 mm. 30 mL 5 mg L^{-1} of aqueous MB are added into a glass petri dish with a diameter of 60 mm. The as-prepared N-doped TiO_2 film (half of the Si wafer, about 10 cm^2) is sunk to the bottom of the petri dish. Before the photoreaction procedures, the system is stirred by magnetic force in the dark for 30 min to ensure the adsorption equilibrium. During the photodegradation process, about 2 mL of the solution is taken at 30 min intervals to a cuvette, and the absorption spectra of the obtained solutions are obtained by UV-vis spectroscopy (UV-3100 PC, VWR).

Results and discussion

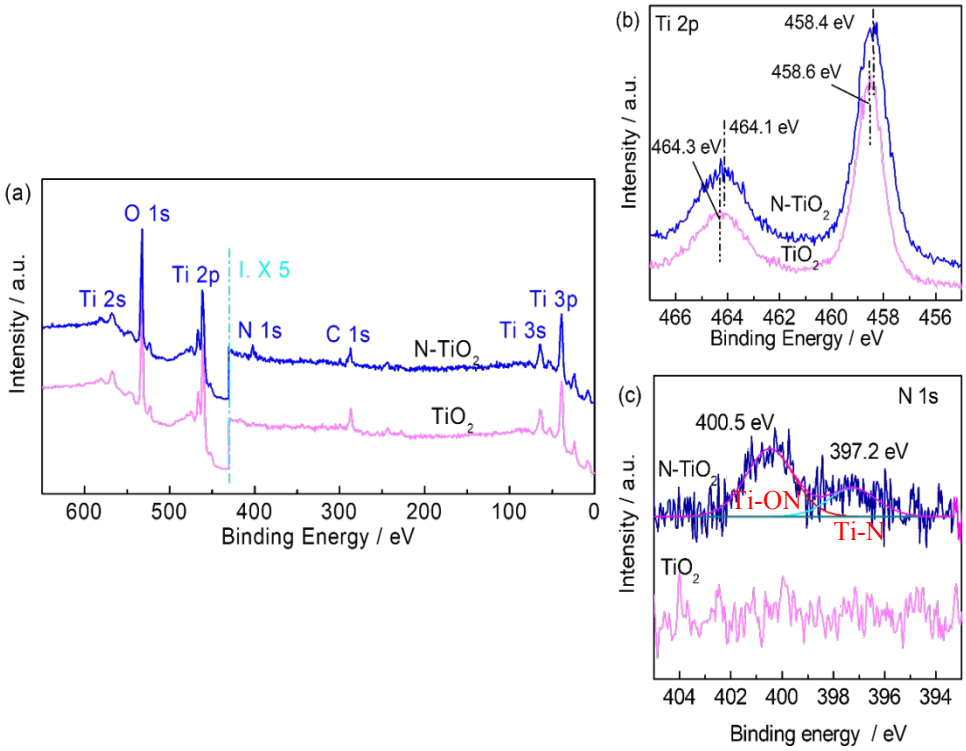

Fig. 2 (a) After sputtered XPS survey spectra and high-resolution spectra of (b) Ti 2p (before sputtering) and (c) N 1s (after sputtering) for TiO_2 and N-TiO_2 coatings treated under 1% NH_3 and 100 W.

The chemical composition of TiO_2 and N-TiO_2 coatings are investigated using XPS survey spectra and high-resolution Ti 2p and N 1s spectra (Fig. 2). After removing the surface contamination by sputtering, for both samples, the survey spectra (Fig. 2(a)) show the presence of O, Ti, and a small amount of C. However, there is a small peak of N 1s in the N-TiO_2 coating, with a 2.64% concentration.

Since sputtering modifies the shape of Ti 2p peaks by reducing Ti^{4+} into Ti^{3+} on the surface, the high-resolution spectra of Ti 2p shown were acquired before sputtering. In Fig. 2(b), the XPS spectrum of the Ti 2P core level obtained from the TiO_2 coating

exhibited a Ti 2p3/2 peak at 458.6 eV and Ti 2p1/2 at 464.3 eV. After treatment in the Ar/NH_3 discharge, the binding energy of Ti 2p3/2 and Ti 2p1/2 of the N-TiO_2 shifts to 458.4 eV and 464.1 eV, respectively. This small shift could be attributed to the electronic interactions of Ti with nitrogen. It is known that the electronegativity of nitrogen is lower than that of oxygen [1,2,8,14]. On the other hand, it has been reported that the incorporation of N atoms into the TiO_2 lattice can also lead to the shift of the Ti 2p peaks to lower binding energies [8]. However, due to the small value of the observed shift (0.2 eV-0.3 eV), which is in the range of the error of the spectrometer, it cannot be accepted as absolute proof for N-doping, as sole.

One of the most interesting results is shown in the N 1s XPS spectra depicted in Fig. 2(c). It shows a complex signal of nitrogen at 400.5 eV and 397.2 eV only in N-TiO_2, which is consistent with the presence of a small N peak in the survey spectra. According to some other recent studies in the same type of conditions [11,12,22,23], the binding energy at 400.5 eV could be assigned to a Ti-O-N structure, characteristic of interstitial N atoms. A variety of peaks with N1s binding energies comprised between 395.8 and 397.8 eV were already found in other works [11,23-25], which are widely regarded as substitutional nitrogen. The variations in the binding energy within this range can be explained by a variation in the oxygen to nitrogen ratio [25,26]. These findings suggest that by the simple atmospheric DBD treatment, N may be introduced in TiO_2 lattices both as the interstitial and substitutional dopant. Similar results on N 1s chemical states of N doped TiO_2 have also been achieved by using an NH_x^+ ion implantation method in a UHV (ultra-high vacuum) chamber at room temperature or at 527 °C [23].

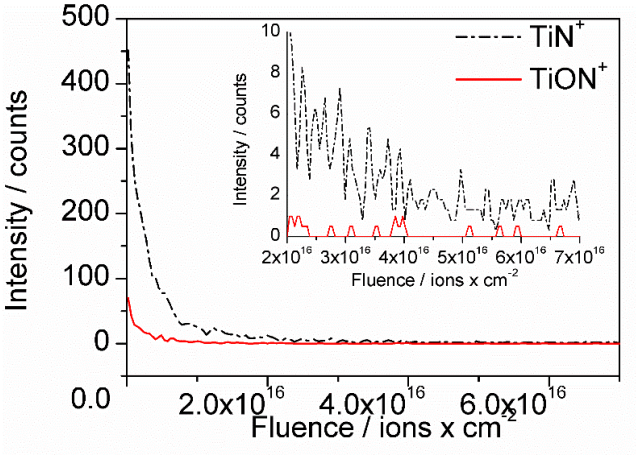

Fig. 3 SIMS depth profiling of N-TiO_2 coating treated under 1% NH_3 and 100 W.

To further prove that nitrogen is present into the TiO_2 lattice, and not just covering the surface, TOF-SIMS depth profiles of the films are performed and presented in Fig. 3. The intensity of different positive ion species is plotted against the Cs^+ sputter fluence for the N-TiO_2 film. A signal attributed to Ti-ON^+ and TiN^+ is observed in the depth profiles, which decreases with higher sputter fluence. These results confirm: (i) nitrogen incorporation into these films in Ti-O-N and Ti-N states and (ii) most of the N is on the surface, especially in the state of Ti-N, while a low amount of Ti-N is distributed through the coating.

However, uncertainty remains on the interstitial or substitutional nature of the doping. The high-resolution N 1s scan (Fig. 2c) shows that most of the nitrogen is interstitial (Ti-ON species) rather than substitutional (N-Ti) from SIMS results (Fig. 3), which is also confusing for us. To our understanding, XPS is more for surface characterization, even after a short time sputtering (in our case 48 s), while SIMS is a depth profiling technique.

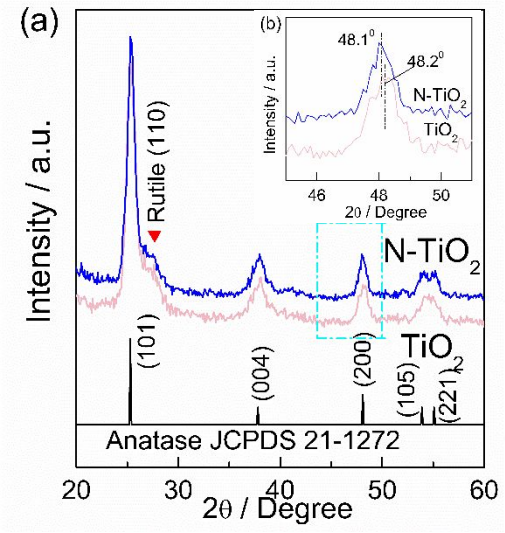

Fig. 4 XRD patterns of TiO_2 and N-TiO_2 coatings treated under 1% NH_3 and 100 W.

Further structural analysis of TiO_2 and N-TiO_2 coatings is carried out using XRD, as presented in Fig. 4(a). With and without N dopant, both films are crystallized in the anatase phase (JCPDS 21-1272) and present a small amount of rutile. It is widely agreed that the biphase structure is preferred to the single phase for charge separation, leading to a higher photocatalytic efficiency [27]. The results suggest that the phase of the TiO_2 coatings does not change with the addition of nitrogen. The inserted figure in Fig. 4b shows the (200) peak position of TiO_2 and N-TiO_2 coatings. A marginal shift of the (200) peak to a smaller degree (higher *d* value) can be noted due to the nitrogen incorporation into the TiO_2 crystal lattice. According to [26,28], a higher *d* value implies compressive residual stress, which may emanate from the differences in the bonding characteristics between nitrogen and oxygen. It might be caused by the N doping when the oxygen is replaced by the nitrogen, resulting in the modification of the electronic states. As a comparison, atmospheric pressure Ar/N_2/H_2 DBD was used to nitride the surface of tool steel by Miyamoto and coworkers [15]. Through the hardness measurement,

they presented the formation of a uniform nitride layer on the steel made the surface hardness increased more than twofold. It was demonstrated that the shift of the XRD pattern was due to the nitrogen atoms solute into the surface of the tool steel.

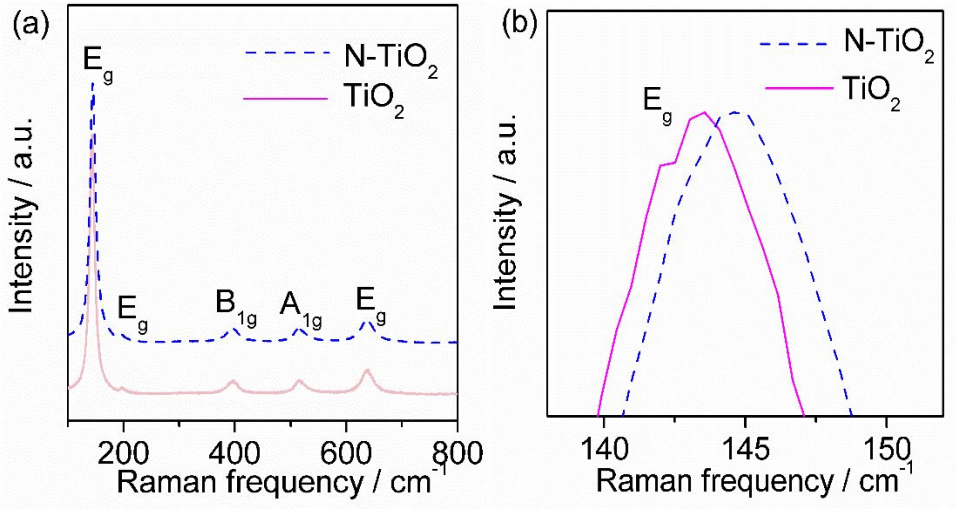

Fig. 5 Raman spectra of TiO_2 and N-TiO_2 coating treated under 1% NH_3 and 100 W.

The phase compositions of TiO_2 and N-TiO_2 coatings are further examined by Raman spectra analysis (Fig. 5a).

Based on the previously reported literature [27], six fundamental transitions are expected in the Raman spectrum of the anatase phase of TiO_2, i.e. 144 cm^{-1} (E_g), 197 cm^{-1} (E_g), 399 cm^{-1} (B_{1g}), 513 cm^{-1} (A_{1g}), 519 cm^{-1} (B_{1g}) and 639 cm^{-1} (E_g). Four Raman bands at 143 cm^{-1} (B_{1g}), 447 cm^{-1} (E_g), 612 cm^{-1} (A_{1g}), and 826 cm^{-1} (B_{2g}) are attributed to the rutile phase. Both the TiO_2 and the N-TiO_2 coatings present the Raman spectra of the anatase phase, with no peaks referring to the rutile phase. However, a small peak is assigned to rutile in the XRD pattern. The absence of the rutile peak in the Raman spectra can be due to the low sensibility of the Raman equipment. Fig. 5(b) shows the enlarged localized profiles of E_g (144 cm^{-1}) peak of the two coatings. The E_g (144 cm^{-}

^{1}) peak slightly shift towards higher wavenumbers from TiO_2 to N-TiO_2. Based on the previous literature, the shift effect is indicative of lattice disorder defects. It can be caused by oxygen vacancies [29,30], the electronic interaction between titania and nitrogen doping [27,31], or the change of the particle size [32,33].

SEM is also therefore employed to characterize the microstructure of the films and to provide more evidence about the shift in Raman spectra. The cross-sectional images of the TiO_2 film and N-TiO_2 film are shown in Fig. 6. Here, it is noteworthy that for TiO_2 and N-TiO_2 films, the mean particle size is 114 ± 2 nm and 116 ± 3 nm, respectively. The average mass loading of the films is about 0.36 mg/cm^2. This result also excludes the hypothesis that the particle size is responsible for the shift in the Raman spectra.

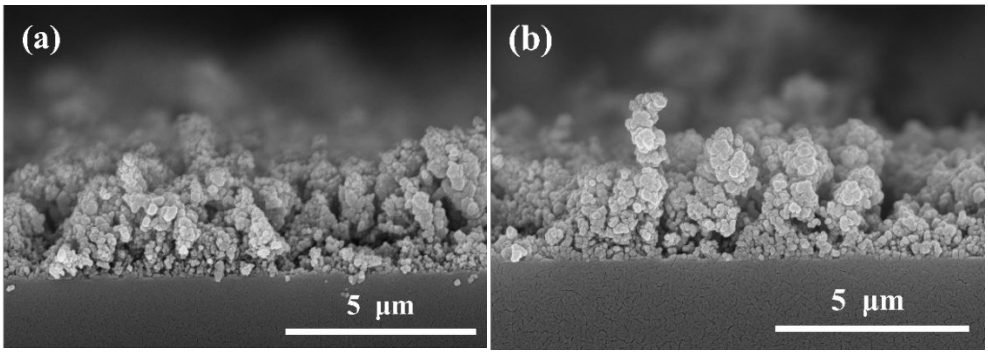

Fig. 6 Cross-sectional SEM images of (a) TiO_2 and (b) N-TiO_2 coatings treated under 1% NH_3 and 100 W.

To evaluate the modification mechanism with the NH_3/Ar mixture plasma, OES is used to diagnose reactive species and uncover the plasma chemical processes in DBD. Two main wavelength ranges are presented in Fig. 7: 300 - 400 nm (Fig. 7a) to study the NH emission spectra and 650 - 900 nm (Fig. 7b) to observe the Ar I emission lines. The peak at 336.0 nm is identified as the NH ($c^1\Pi(v = 0)$) → $X^3\Sigma(v = 1)$ radical, while the

peak at 337.1 nm is identified as the NH ($A^3\Pi(v = 1)) \rightarrow X^3\Sigma(v = 1)$ as well as the second positive system (SPS $C^3\Pi_u \rightarrow B^3\Pi_g$) of N_2 [16,34]. Compared with the spectra of the pure argon plasma, NH radicals at 336.0 nm obviously appear in the spectra of the Ar/NH_3 plasma (shown in Fig. 7a). The peak of N_2 at 337.1 nm appears in both spectra, and originates from air contamination. In NH_3/Ar plasma Fig. 7b, the intensity of Ar I at 763.51 nm and 811.53 nm indexed to $2p_6 \rightarrow 1s_5$, $2p_9 \rightarrow 1s_5$ (Paschen notation of the terms) transitions, respectively, which contributed to the Ar metastable states, relatively decrease compared with pure Ar plasma. In addition, other fraction productions like N_2^+ radicals which shows a peak at 387.6 nm, possibly also partially contribute to the introduction of nitrogen group in the coating.

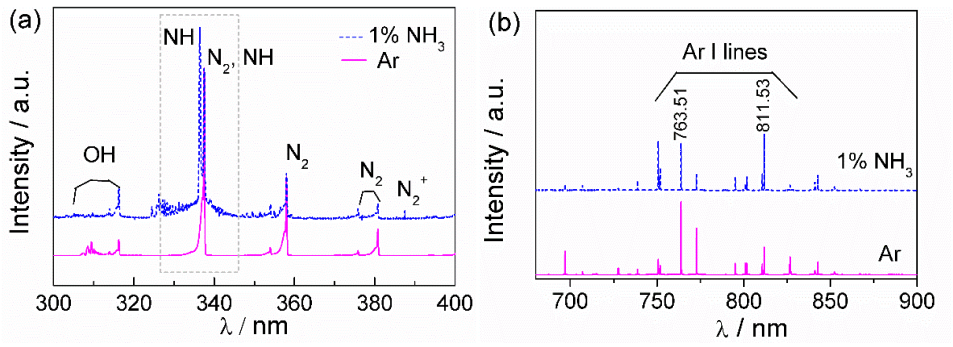

Fig. 7 Optical emission spectra of plasma with 1% and without NH_3 under 100 W in (a) 300-400 nm and in (b) 650-900 nm range.

The analysis assumes that the NH radicals are generated by electron driven collisional excitation, ionization reactions and Penning ionization with subsequent quenching effect. Chemical reactions between argon metastable atoms and ammonia molecules, including the collisional excitation and ionization reactions, Penning reactions and quenching as detailed below [16,34,35].

Collisional excitation and ionization reactions:

$e^- + NH_3 \rightarrow NH_3^* + e^-$ (1)

$e^- + NH_3 \rightarrow NH + 2H + e^-$ (2)

$e^- + NH_3^* \rightarrow NH + 2H + e^-$ (3)

$e^- + NH_3 \rightarrow NH_3^+ + 2e^-$ (4)

$e^- + NH_3^* \rightarrow NH_3^+ + 2e^-$ (5)

Penning reactions:

$Ar\ (^3P_2, ^3P_0) + NH_3 \rightarrow NH_3^+ + Ar + e^-$ (6)

$\rightarrow NH_2 + Ar + H$ (7)

$\rightarrow NH + Ar + H + H$ (8)

Three-body and Binary reactions:

$NH_2 + H + Ar \rightarrow Ar + NH_3$ (9)

$NH_2 + NH_2 + Ar \rightarrow Ar + N_2H_4$ (10)

$NH + H + H + Ar \rightarrow Ar + NH_3$ (11)

$H + H + Ar \rightarrow Ar + H_2$ (12)

$NH + NH \rightarrow 2H + N_2$ (13)

$NH + H \rightarrow N + H_2$ (14)

$NH_2 + N \rightarrow 2H + N_2$ (15)

On top of the three-body and binary reactions listed above, direct quenching of NH by NH_3 is also presented, as already reported by B. Gelernt and S.V. Filseth. [36]

The introduction of N into TiO_2 coatings may be related to the concentration of NH radicals in the plasma. For further analysis, the effect of the concentration of NH_3 and

the applied power are investigated and presented in Fig. 8. It is shown in Fig. 8(a) that an increase of NH_3 concentration at a fixed power (100 W) leads to a decrease of the NH content. A similar trend was reported by A. Fateev and co-workers [16] and Z. Chang and coworkers [34]. A. Fateev and coworkers explained this effect by the electronegativity of NH_3. Electron capture by ammonia molecules lead to the formation of H^- and NH_2^- negative ions [16] that reduced the formation of NH. Z. Chang and coworkers [34] interpreted this phenomenon with the Penning effect and the quenching effect of NH_3. The Penning effect between the Ar metastable and the NH_3 molecule dominates the discharge property. However, the quenching effect of the surplus NH_3 mainly influences the discharge when the concentration of NH_3 is high [34]. An increase in applied power leads to a more efficient ammonia decomposition [16], which causes the increase of the NH signal as shown in Fig. 8b. One can notice that the concentration of N in the TiO_2 coatings (based on the XPS results after sputtering) decreases as the relative intensity of NH decreases (based on the OES results). This suggests that the NH radical concentration in the plasma contributes to the doping of the TiO_2 coatings. It was reported that the NH radical may have a higher probability to form a covalent bond or to induce defects on MWCNTs [19]. B.S. Truscott and coworkers [37] also reported that NH radicals played a crucial role in the deposition of nitrogen-doped diamond by microwave plasma-activated CVD. Recently, Ciolan and coworkers [38] investigated Ar/NH_3 gas mixture plasmas processing onto the RF magnetron-sputtered defective ZnO thin films. They claimed that the concentration of NH in the plasma was maximum at a small amount of NH_3 gas, which is determined from the product of NH_3

concentrations and electron density. The similar results were obtained by Oever and coworkers. [39]

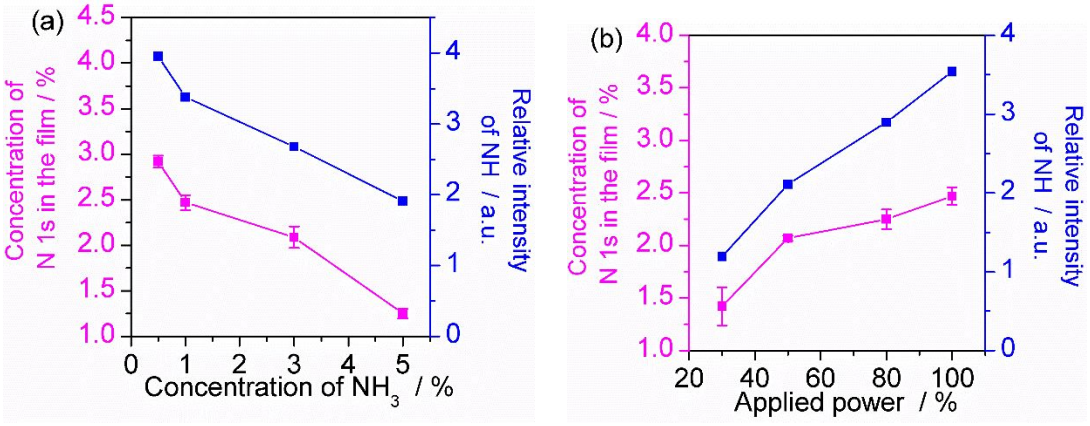

Fig. 8 Intensity of the OES NH radical line (336.0 nm) and concentration of N1s in the TiO_2 films as a function of (a) different concentrations of NH_3, while the flow rate of Ar is 2 slm and the applied power is 100 W; (b) different applied power, while the concentration of NH_3 is 1%, and the flow rate of Ar is 2 slm.

To determine the effect of nitrogen doped TiO_2 on the UV-vis light response, we further studied the optical property of the coatings with UV-vis spectroscopy. The UV-vis DRS spectra of the TiO_2 coatings are shown in Fig. 9. The comparison of the spectrum of the TiO_2 coating and the spectrum of the N-TiO_2 coating reveals a red shift of the absorption edge toward the visible region for N-TiO_2 coating (Fig. 9a), as it was reported by previous works [1,2,14,40,41]. This is attributed to the presence of nitrogen atoms in the TiO_2 lattices, leading to the appearance of N2p inter-band energy levels in the TiO_2 band gap just above the upper edge of the valence band.

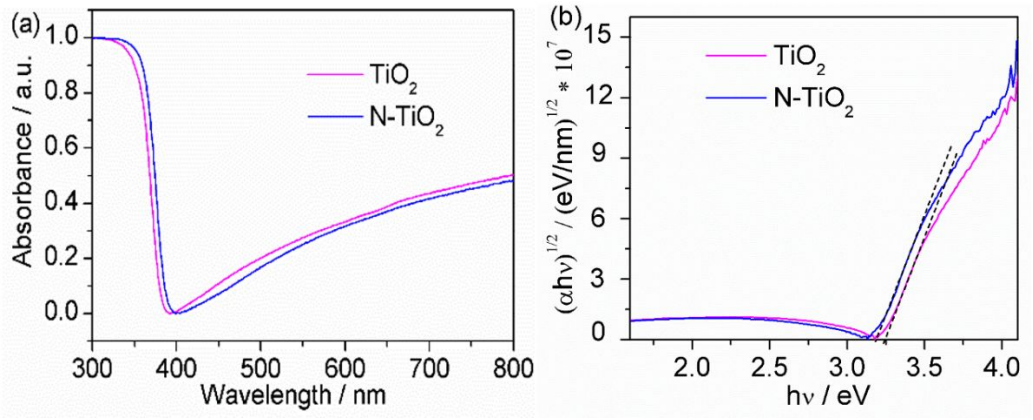

Fig. 9 UV-vis diffuse reflectance spectra (DRS) of undoped (purple curve) and N-doped (blue curve) TiO_2 coating treated under 1% NH_3 and 100 W (a) and the corresponding $(\alpha h\nu)^{1/2}$ versus $h\nu$ plots used to determine the optical band gaps (b).

The band gaps of the TiO_2 and N-TiO_2 is estimated by using Tauc plots [2,42], as shown in Fig. 9(b). To do this, $(\alpha h\nu)^{1/2}$ vs $h\nu$ is plotted according to the equation:

$$(\alpha h\nu)^{1/2} = k\,(h\nu - E_g),$$

where α is the absorption coefficient and $h\nu$ is the photon energy, k is a constant, E_g is band gap. The absorption coefficient is estimated from the equation:

$$\alpha = \frac{1}{d} \cdot \ln\left[\frac{1-R^2}{T(\lambda)}\right],$$

where d is the thickness, R is the reflectance, $T(\lambda)$ is the transmittance of the film. The linear portion of the Tauc plot intersects the X-axis at $(\alpha h\nu)^{1/2} = 0$. The values of E_g have been estimated from this intercept [43,44]. As calculated, the band gap of the N-TiO_2 coating is 3.18 eV and that of the undoped TiO_2 coatings is 3.25 eV. This supports the proof that the NH_3/Ar plasma treatment reduces the band gap of TiO_2.

The photocatalytic performance of TiO_2 and N-TiO_2 coatings have been carried out by degrading MB under white LED light irradiation. Fig. 10a illustrates the degradation of

MB as a function of irradiation time in the presence of TiO_2 and N-TiO_2 films and the control experiment. It shows that in the absence of the catalysts, MB is subjected to photolysis resulting in the decrease of the absorbance after 180 min irradiation. The MB degradation with the TiO_2 coating reaches 34% after 180 min irradiation. Compared with the TiO_2 coating, the catalytic efficiency of N-TiO_2 is evidently enhanced with 43% degradation in the same conditions. The linear relationship of $\ln(C/C_0)$ versus time (Fig. 10b) suggests that the photocatalytic degradation of MB solution follows pseudo-first-order kinetics. The photocatalytic degradation rate constant for N-TiO_2 coating is 0.187 h^{-1}, about 1.4 times higher than that of the undoped TiO_2 coating (0.137 h^{-1}). This result further confirms a successful plasma treatment on the enhancement of the N-TiO_2 coatings photocatalytic activity.

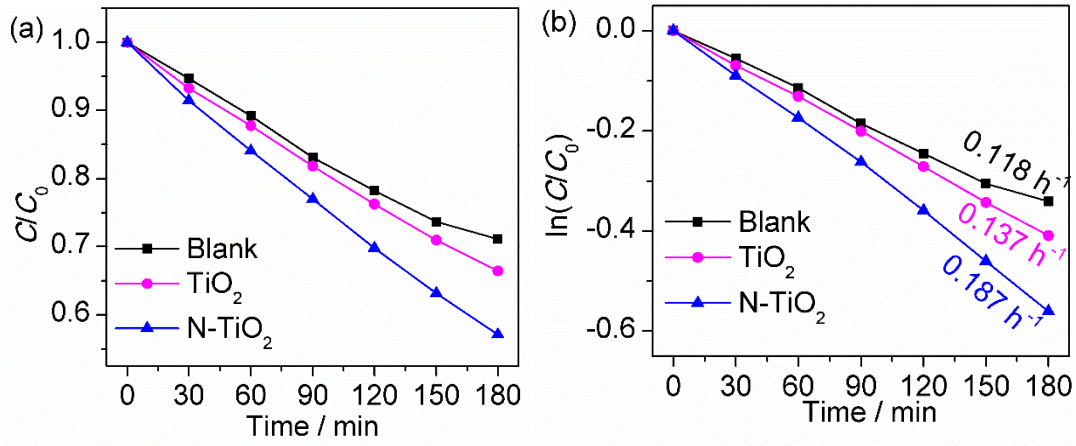

Fig. 10 Relative concentration curves of MB aqueous solutions (initial concentration: 5 mM/L) upon different experimental conditions under the white LED irradiation (a) and the first-order kinetics (b).

Conclusion

This study reports the simple, fast and efficient nitrogen doping of TiO_2 coating using a room temperature NH_3/Ar DBD operating at atmospheric pressure. XPS and SIMS

results indicate a nitrogen doping of the TiO_2 lattice. Uncertainty remains on the interstitial or substitutional nature of the doping, as XPS suggests TiON and SIMS TiN. Binding energy shifts in XPS (for Ti 2p), wavenumber shifts in Raman, and diffraction angle in XRD, all suggest nitrogen incorporation in the TiO_2 matrix. All these shifts are in the error range of the respective technique and they can therefore not be taken as solid and robust evidence for doping. However, XPS data show that nitrogen is effectively incorporated into the TiO_2 matrix, up to a few percents. This is confirmed by SIMS depth profiling and a change in photocatalytic activity. Both techniques also reveal the presence (in variable amounts) of TiON and TiN components, reinforcing the evidence for doping. The doping mechanism is investigated by OES to study the plasma properties under different conditions. It suggests that the NH radicals play a key role in the TiO_2 doping. The concentration of nitrogen in the N-TiO_2 coatings can be adapted by changing the concentration of NH_3 in the plasma or the applied power. The bandgap of N-TiO_2 is significantly reduced after the NH_3/Ar plasma treatment from 3.25 to 3.18 eV. The N-TiO_2 coating shows highly enhanced photocatalytic activity under white LED irradiation. Indeed, the photocatalytic degradation rate constant for N-TiO_2 coating is improved more than 1.4 times compared with the undoped TiO_2 coating.

Acknowledgments

The authors would like to thank the China Scholarship Council (CSC, Grant no. 201407040053) for a PhD scholarship (Q. Chen) and the Belgian Federal Office for Science Policy (BELSPO) for its financial support through the IAP-VII/12, P7/34 (Interuniversity Attraction Pole) program 'PSI-Physical Chemistry of Plasma Surface Interactions'. The FNRS/FWO EoS (Excellence of Science) project NITROPLASM also contributed to funding this research. B. C. kindly acknowledges financial support from the FRS-FNRS (Belgian National Scientific Research Fund) for the POLYGRAD Project 22333186. B. C. is an FRS-FNRS Research Fellow.

References

[1]. Fujishima, A.; Honda, K.; Electrochemical Photolysis of Water at a Semiconductor Electrode, *Nature* **1972**, *238*, 37-38.

[2]. Islam, S. Z.; Reed, A.; Wanninayake, N.; Kim, D. Y.; Rankin, S. E.; Remarkable Enhancement of Photocatalytic Water Oxidation in N_2/Ar Plasma Treated, Mesoporous TiO_2 Films, *J. Phys. Chem. C* **2016**,*120*, 14069-14081.

[3]. Patil K., M.; Shaikh, S.; Ganesh, I.; Recent Advances on TiO_2 Thin Film Based Photocatalytic Applications (A Review), *Curr. Nanosci.* **2015**, *11*, 271-285.

[4]. Roose, B.; Pathak, S.; Steiner, U.; Doping of TiO_2 for Sensitized Solar Cells, *Chem. Soc. Rev.* **2015**, *44*, 8326-8349.

[5]. Asahi, R.; Morikawa, T.; Ohwaki, T.; Aoki, K.; Taga, Y.; Visible-light

Photocatalysis in Nitrogen-Doped Titanium Oxides, *Science* **2011**, *293*, 269-271.

[6]. Sathish, M.; Viswanathan, B.; Viswanath, R. P.; Gopinath, C. S.; Synthesis, Characterization, Electronic Structure, and Photocatalytic Activity of Nitrogen-Doped TiO_2 Nanocatalyst, *Chem. Mater.* **2005**, *17*, 6349-6353.

[7]. Ansari, S. A.; Khan, M. M.; Ansari, M. O.; Cho, M. H.; Nitrogen-doped Titanium Dioxide (N-doped TiO_2) for Visible Light Photocatalysis, *New J. Chem.* **2016**, *40*, 3000-3009.

[8]. Wang, J.; Tafen, D. N.; Lewis, J. P.; Hong, Z.; Manivannan, A.; Zhi, M.; Li, M.; Wu, N.; Origin of Photocatalytic Activity of Nitrogen-Doped TiO_2 Nanobelts, *J. Am. Chem. Soc.* **2009**, *131*, 12290-12297.

[9]. Yang, G.; Jiang, Z.; Shi, H.; Xiao, T.; Yan, Z.; Preparation of Highly Visible-Light Active N-Doped TiO_2 Photocatalyst, *J. Mater. Chem.* **2010**, *20*, 5301-5309.

[10]. Romero-Gomez, P.; Hamad, S.; Gonzalez, J. C.; Barranco, A.; Espinos, J. P.; Cotrino, J.; Gonzalez-Elipe, A. R.; Band Gap Narrowing versus Formation of Electronic States in the Gap in N-TiO_2 Thin Films, *J. Phys. Chem. C* **2010**, *114*, 22546-22557.

[11]. Stegemann, C.; Moraes, R.S.; Duarte, D.A.; Massi, M.; Thermal Annealing Effect on Nitrogen-Doped TiO_2 Thin Films Grown by High Power Impulse Magnetron Sputtering Plasma Power Source, *Thin Solid Films* **2017**, *625*, 49-55.

[12]. Sahoo, M.; Mathews, T.; Antony, R. P.; Krishna, D.N.; Dash, S.; Tyagi, A. K.; Physicochemical Processes and Kinetics of Sunlight-Induced Hydrophobic-Superhydrophilic Switching of Transparent N-Doped TiO_2 Thin Films, *ACS Appl.*

Mater. Interfaces **2013**, *5*, 3967-3974.

[13]. Kosowska, B.; Mozia, S.; Morawski, A. W.; Grzmil, B.; Janus, M.; Kaucki, K.; The Preparation of TiO_2–Nitrogen Doped by Calcination of TiO_2•xH_2O under Ammonia Atmosphere for Visible Light Photocatalysis, *Sol. Energy Mater. Sol. Cells* **2005**, *88*, 269–280.

[14]. Li, B.; Zhao, Z.; Zhou, Q.; Meng, B.; Meng, X.; Qiu, J.; Highly Efficient Low-Temperature Plasma-Assisted Modification of TiO_2 Nanosheets with Exposed {001} Facets for Enhanced Visible-Light Photocatalytic Activity, *Chem. Eur. J.* **2014**, *20*, 14763-14770.

[15]. Miyamoto, J.; Inoue, T.; Tokuno, K.; Tsutamori, H.; Abraha, P.; Surface Modification of Tool Steel by Atmospheric-Pressure Plasma Nitriding Using Dielectric Barrier Discharge, *Tribology online* **2016**, *11*, 460-465.

[16]. Fateev, A.; Leipold, F.; Kusano, Y.; Stenum, B.; Tsakadze, E.; Bindslev, H.; Plasma Chemistry in an Atmospheric Pressure Ar/NH_3 Dielectric Barrier Discharge, *Plasma Process. Polym.* **2005**, *2*, 193–200.

[17]. Kyzioł, K.; Koper, K.; Kaczmarek, Ł.; Grzesik, Z.; Plasmochemical Modification of Aluminum-Zinc Alloys Using NH_3-Ar Atmosphere with Anti-Wear Coatings Deposition, *Mater. Chem. Phys.* **2017**, *189*, 198-206.

[18]. Pulsipher, D. J. V.; Fisher, E. R.; NH_2 and NH Surface Production in Pulsed NH_3 Plasmas on TiO_2: A Steady-State Probe of Short Pulse Plasmas, *Plasma Process. Polym.* **2013**, *10*, 6-18.

[19]. Chen, C.; Liang, B.; Lu, D.; Ogino, A.; Wang, X.; Nagatsu, M.; Amino Group

Introduction onto Multiwall Carbon Nanotubes by NH_3/Ar Plasma Treatment, *Carbon* **2010**, *48*, 939-948.

[20]. Chen, Q.; Liu, Q.; Ozkan, A.; Chattopadhyay, B.; Wallaert, G.; Baert, K.; Terryn, H.; Delplancke-ogletree, M.-P.; Geerts, Y. H.; Reniers, F.; Atmospheric Pressure Dielectric Barrier Discharge Synthesis of Morphology-Controllable TiO_2 Films with Enhanced Photocatalytic Activity, *Thin Solid Films* **2018**, *664*, 90-99.

[21]. Wu, D.; Wang, W.; Ng, T. W.; Huang, G.; Xia, D.; Yip, H. Y.; Lee, H. K.; Li, G.; An, T.; Wong, P. K.; Visible-Light-Driven Photocatalytic Bacterial Inactivation and Mechanism of Zinc Oxysulfide under LED Light Irradiation, *J. Mater. Chem. A* **2016**, *4*, 1052-1059.

[22]. Georgieva, J.; Valova, E.; Armyanov, S.; Tatchev, D.; Sotiropoulos, S.; Avramova, I.; Dimitrova, N.; Hubin, A.; Steenhaut, O.; A Simple Preparation Method and Characterization of B and N Co-Doped TiO_2 Nanotube Arrays with Enhanced Photoelectrochemical Performance, *Appl. Surf. Sci.* **2017**, *413*, 284-291.

[23]. Kim, Y. K.; Park, S.; Kim, K.; Kim, B.; Photoemission Study of N-Doped TiO_2 (110) with NH_3, *J. Phys. Chem. C* **2011**, *115*, 18618-18624.

[24]. Palgrave, R. G.; Payne, D. J.; Egdell, R. G.; Nitrogen Diffusion in Doped TiO_2 (110) Single Crystals: A Combined XPS and SIMS Study, *J. Mater. Chem.* **2009**, *19*, 8418-8425.

[25]. Glaser, A.; Surnev, S.; Netzer, F. P.; Fateh, N.; Fontalvo, G. A.; Mitterer, C.; Oxidation of Vanadium Nitride and Titanium Nitride Coatings, *Surf. Sci.* **2007**, *601*, 1153-1159.

[26]. Yang, X.; Cao, C.; Erickson, L.; Hohn, K.; Maghirang, R.; Klabunde, K.; Photo-catalytic Degradation of Rhodamine B on C-, S-, N-, and Fe-doped TiO_2 under Visible-Light Irradiation, *Appl. Catal., B: Environ.* **2009**, *91*, 657-662.

[27]. Preethi, L. K.; Antony, R. P.; Mathews, T.; Walczak, L.; Gopinath, C. S.; A Study on Doped Heterojunctions in TiO_2 Nanotubes: An Efficient Photocatalyst for Solar Water Splitting, *Sci. Rep.* **2017**, *7*, 14314-1-15.

[28]. Jagadale, T. C., Takale, S. P.; Sonawane, R. S.; Joshi, H. M.; Patil, S. I.; Kale B. B.; Ogale, S. B.; N-Doped TiO_2 Nanoparticle Based Visible Light Photocatalyst by Modified Peroxide Sol-Gel Method, *J. Phys. Chem. C*. **2008**, *112*, 14595-14602.

[29]. Naldoni, A.; Allieta, M.; Santangelo, S.; Marelli, M.; Fabbri, F.; Cappelli, S.; Bianchi, C. L.; Psaro, R.; Santo, V. D.; Effect of Nature and Location of Defects on Bandgap Narrowing in Black TiO_2 Nanoparticles, *J. Am. Chem. Soc.* **2012**, *134*, 7600-7603.

[30]. Kim, C.; Kim, K.-S.; Kim, H. Y.; Han, Y. S.; Modification of a TiO_2 Photoanode by Using Cr-Doped TiO_2 with an Influence on the Photovoltaic Efficiency of a Dye-Sensitized Solar Cell, *J. Mater. Chem.* **2008**, *18*, 5809-5814.

[31]. Melvin, A. A.; Illath, K.; Das, T.; Raja, T.; Bhattacharyya S.; Gopinath C. S.; M-Au/TiO_2 (M = Ag, Pd, and Pt) Nano Photocatalyst for Overall Solar Water Splitting: Role of Interfaces, *Nanoscale* **2015**, *7*, 13477-13488.

[32]. Choi, H. C.; Jung, Y. M.; Kim, S. B.; Size Effects in the Raman Spectra of TiO_2 Nanoparticles, *Vib. Spectrosc.* **2005**, *37*, 33-38.

[33]. Zhang, W. F.; He, Y. L.; Zhang, M. S.; Yin, Z.; Chen, Q.; Raman Scattering

Study on Anatase TiO_2 Nanocrystals, *J. Phys. D: Appl. Phys.* **1999**, *33*, 912-916.

[34]. Chang, Z.; Yao, C.; Chen, S.; Zhang, G.; Electrical and Optical Properties of Ar/NH_3 Atmospheric Pressure Plasma Jet, *Phys. Plasmas* **2016**, *23*, 093503-1-9.

[35]. Sarani, A.; Nikiforov, A.; Leys, C.; Atmospheric Pressure Plasma Jet in Ar and Ar/H_2O Mixtures: Optical Emission Spectroscopy and Temperature Measurements, *Phys. Plasmas* **2010**, *17*, 063504-1-9.

[36]. Gelernt, B.; Filseth, S. V.; Carrington, T.; Quenching and Radiative Lifetimes for NH (b1Σ+, υ′ = 0), Chem. Phys. Lett. **1975**, *36(2)*, 238-241.

[37]. Truscott, B. S.; Kelly, M. W.; Potter, K. J.; Johnson, M.; Ashfold, M. N. R.; Mankelevich, Y.A., Microwave Plasma-Activated Chemical Vapor Deposition of Nitrogen-Doped Diamond. I. N_2/H_2 and NH_3/H_2 Plasmas, *J. Phys. Chem. A* **2015**, *119*, 12962-12976.

[38]. Ciolan, M.A.; Motrescu, I.; Sugiura, K.; Luca, D.; Nagatsu, M.; Tailoring the Surface Functionalities of Radio Frequency Magnetron-Sputtered ZnO Thin Films by Ar/NH_3 Gas Mixture Surface-Wave Plasmas, *Langmuir* **2018**, *34(38)*, 11253-11263.

[39]. Van den Oever, P. J.; Van Helden, J. H.; Lamers, C. C. H.; Engeln, R.; Schram, D. C.; Van de Sanden, M. C. M.; Kessels, W.M.M.; Density and Production of NH and NH_2 in an Ar-NH_3 Expanding Plasma Jet, *J. Appl. Phys.* **2005**, *98*, 093301-093310.

[40]. Irie, H.; Watanabe, Y.; Hashimoto, K.; Nitrogen-Concentration Dependence on Photocatalytic Activity of $TiO_{2-x}N_x$ Powders, *J. Phys. Chem. B* **2003**, *107*, 5483-

5486.

[41]. Buha, J.; Optical Properties and Structure of the TiN-Nitrogen-Doped TiO_2 Nanocomposite, *Appl. Surf. Sci.* **2014**, *321*, 457-463.

[42]. Valencia, S.; Marín, J. M.; Restrepo, G.; Study of the Bandgap of Synthesized Titanium Dioxide Nanoparticules Using the Sol-Gel Method and a Hydrothermal Treatment, *Open Mater. Sci*. J. **2010**, *4*, 9-14.

[43]. Grigorov, K. G.; Oliveira, I. C.; Maciel, H. S., Massi, M.; Oliveira, M. S., Amorim, J.; Cunha, C. A.; Optical and Morphological Properties of N-doped TiO_2 Thin Films, *Surf. Sci.* **2011**, *605*, 775-782.

[44]. Hassanien, A.S.; Akl, A. A.; Influence of Composition on Optical and Dispersion Parameters of Thermally Evaporated Non-Crystalline $Cd_{50}S_{50-x}Se_x$ Thin Films, *J. Alloy. Compound.* **2015**, *648*, 280-290.

Table of Contents Graphic